Touchdown of Flying Recording Head Sliders on Continuous and Patterned Media

Jia-Yang Juang and Kuan-Te Lin

Department of Mechanical Engineering, National Taiwan University, Taipei 10617, Taiwan

We conduct three-dimensional transient finite-element analysis to study the contact behavior during touchdown detection by a thermal flying-height control (TFC) recording head on continuous and patterned elastic-plastic layered media. The heat generated during touchdown and the plastic strain of the media are calculated in the model. We investigated key factors such as the radius of curvature of the TFC protrusion, media compositions, bit-patterned media (BPM), and the effect of planarization. Our analysis shows that when subjected to the same TFC over-push, BPM is much more likely to result in plastic deformation than the continuous media. The temperature distribution of planarized BPM with SiO_2 as filling material exhibits a complex and distinctive pattern different from the one without planarization. More importantly, the maximum plastic strain of the planarized BPM is 50% larger than the one without planarization, which means that filling with SiO_2 deteriorates the media's robustness to the touchdown probably due to the mismatch of thermal properties between SiO_2 and recording material. This suggests the filling material must be carefully chosen to avoid the excessive plastic strain.

***Index Terms*—Head-disk interface (HDI), magnetic recording, patterned media, thermal flying-height control (TFC), touchdown.**

I. Introduction

THERMAL flying height control (TFC) sliders using thermal actuation have been widely used to increase the areal recording density by flying magnetic recording heads in close proximity of magnetic media in hard disk drives (HDDs). In order to further minimize the head-media clearance, a TFC "touchdown (TD) and pull-back (PB)" scheme has been implemented [1]. The operation of touchdown and pull-back is performed by thermally protruding a small portion of the head into contact with the disk, and then backing it off to achieve a desired clearance. The accuracy and repeatability of contact detection is crucial to a reliable head-disk interface (HDI) since it determines the minimum clearance that can be set. Acoustic emission (AE) and laser Doppler Vibrometery (LDV) have been routinely used to detect the onset of touchdown by detecting elastic wave and vibration generated during touchdown [2]–[7]. While these methods in general can detect touchdown with good sensitivity on a spin stand, they cannot be used in hard disk drives. Some detection methods used in drive level are change of spindle motor current, change of flexible cable bias and position-error signal (PES). These methods indirectly measure the friction generated during TFC touchdown.

Bit-patterned media (BPM) is considered as a revolutionary technology to extend recording densities beyond limitations imposed by the onset of the superparamagnetic effect in conventional continuous media [8], [9]. However, the fabrication of isolated nanometer islands can further stress the tribology of head-disk interfaces due to poorer contact detection and material robustness. Planarization of the BPM is proposed to avoid potential dynamic instability induced by flying air-bearing slider on a patterned surface. Nunez *et al.* studied the contact behavior of planarized patterned media using a two-dimensional finite-element model, and concluded that no significant difference was observed between a stiffer filling material and a softer one [10]. Since frictional heating was not included in their model, it is still not clear how the touchdown process may impact the thermal-mechanical robustness of the BPM when frictional heating and thermal properties are considered.

In this paper, we conduct three-dimensional (3-D) transient finite-element analysis to study the contact behavior during touchdown detection on continuous media, unplanarized BPM, and BPM planarized with SiO_2. We analyze the friction, frictional heating, temperature rise, and media plastic deformation, and investigate the effect of planarization.

II. Modeling

A. TFC Bulge and Touch-Down Process

The TFC bulge (or protrusion profile) depends on various design parameters, such as heater design, head structure and air-bearing design, as well as environmental conditions, such as altitude, gas types, and humidity [11]–[16]. Its radius of curvature R also depends on the heating power applied to the heating element. The prediction of the bulge involves a complicated model, which couples the head and the air-bearing. The bulge radius of some commercial TFC sliders is about 2 mm [1]. In this paper, we assume the bulge is spherical and rigid, and its radius ranges from 500 μm to 2 mm.

The touchdown process is modeled as a quasi-static indentation (or over-push) and a fast sliding of the bulge on the media. The indentation is simulated by moving the bulge into contact with the media while the media is stationary, and the sliding is simulated by displacing the bulge at a constant tangential velocity V with respect to the media. The onset of touchdown is defined at zero clearance between the bulge and the media, and the over-push δ is the distance the bulge moves toward the media after the touchdown.

B. Frictional Heating

Coulomb friction is used to model the sliding at the contact interface between the bulge and media. A coefficient of friction

Manuscript received December 01, 2012; revised February 07, 2013; accepted February 13, 2013. Date of current version May 30, 2013. Corresponding author: J.-Y. Juang (e-mail: jiayang@ntu.edu.tw).

Color versions of one or more of the figures in this paper are available online at http://ieeexplore.ieee.org.

Digital Object Identifier 10.1109/TMAG.2013.2249054

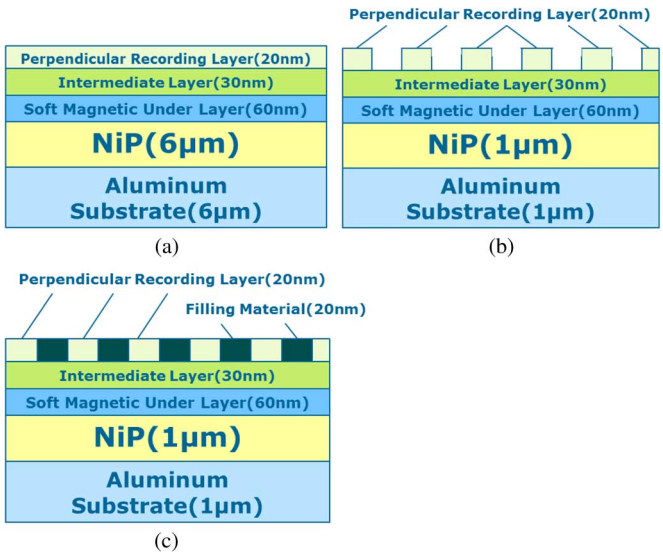

Fig. 1. Schematic of the layered media stacks (not to scale). (a) Continuous media. (b) Bit-patterned media without planarization. (c) Bit-patterned media with planarization.

of 0.2 is used for all simulations. During TFC touchdown energy generated in the form of heat within the contact region due to friction results in temperature rise, which in turn develops thermal stresses and variations of real contact area and contact pressure distribution due to thermal expansion. The thermal and mechanical stress fields are fully coupled, and mechanical equilibrium and thermal equilibrium must be satisfied. Assuming that all mechanical work during the contact is dissipated as heat, the frictional heat q (W/m^2) is given by

$$q = \mu p V \tag{1}$$

where μ is the coefficient of friction, p is the time-dependent contact pressure, and V is the sliding velocity. We assume that the interface thermal resistance of the bulge and media contact pair is negligible, which means the temperature is continuous across the contact interface, and as a result the heat generated by friction transfers to the bulge and media according to their respective thermal properties.

C. Finite-Element Model

Fig. 1(a)–(c) shows the schematics of media stacks of the continuous media, unplanarized BPM, and planarized BPM, respectively. The media model includes detailed layered structures. All commercial media have a diamond-like carbon overcoat (DLC) and a lubricant monolayer on top of the recording layer. Those layers are crucial to a reliable HDI since the DLC minimizes wear and the lubricant reduces friction when head-disk occurs. The thickness of those layers is on the order of one to three nanometers each. We do not explicitly include them in our model, but lump them together with the recording layer. The coefficient of friction used in this paper is based on measurements of samples with DLC and lubricant. The recording layer's material properties, however, are not adjusted.

We carry out 3-D transient finite-element analysis using commercial software package LS-DYNA [17], which solves the momentum equation by explicit time integration, and solves the thermal equilibrium equation by implicit time integration using backward integration [18].

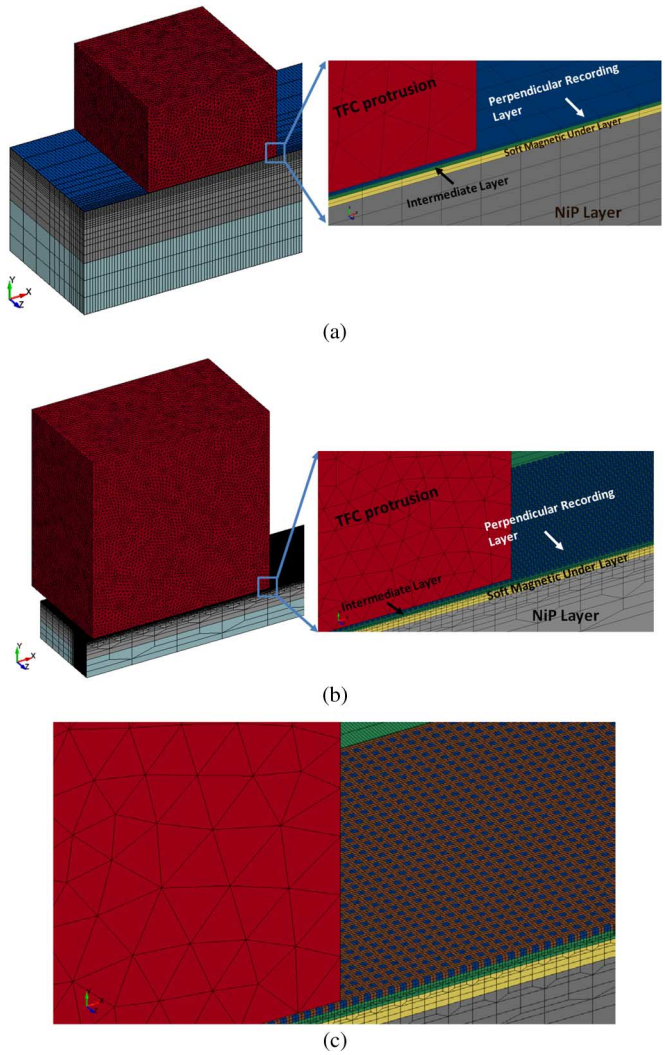

Fig. 2. Finite-element models for (a) continuous media. (b) Bit-patterned media without planarization. (c) Bit-patterned media with planarization.

Fig. 2(a)–(c) shows 3-D finite-element models of the bulge in contact with the thermal-elastic-plastic layered continuous media, BPM, and planarized BPM, respectively. Since the bulge is assumed to be rigid, only a portion of it is modeled, and the contact surface has a radius of curvature R. Due to symmetry with respect to the xy plane only one-half of the bulge and the media are modeled. In order to obtain accurate results we mesh the bulge and the media with increasingly finer mesh near the contact region, whereas region away from the contact region is meshed with coarser mesh to reduce computation time. Mesh convergence studies are performed to ensure the current mesh is balanced between accuracy and computation time. Symmetry boundary conditions are applied at the xy plane. The bottom of the media is constrained in the x, y, and z directions, and is kept at 300 K. The bulge and media is set at a uniform initial temperature of 300 K.

The BPM consists of regularly spaced isolated square islands as shown in Fig. 2(b). The islands have a constant height of 20 nm and a pitch of 40 nm. The planarization of the BPM is achieved by filling the space between islands with SiO_2, and the

TABLE I
NOMINAL MECHANICAL AND THERMAL MATERIAL PROPERTIES OF SLIDER, GLASS AND ALUMINUM (Al-Mg) SUBSTRATES, NiP LAYER, CoFe BASED SOFT MAGNETIC UNDERLAYER (SMUL), Ru BASED INTERMEDIATE LAYER (IL), CoCrPt BASED PERPENDICULAR RECORDING LAYER (PMR)

Property	Symbol [units]	Slider	SiO_2	Al-Mg	Nip	SMUL CoFe	IL RU	PMR CoCrPt
Young's modulus	E [GPa]	400.0	75	71.0	114.0	120.0	135.0	150
Yield strength	Y [GPa]	6.4	-	0.67	3.00	3.7	3.90	3.4
Poisson's ratio	ν [-]	0.3	0.17	0.33	0.31	0.30	0.30	0.3
Density	ρ [kg/m^3]	4300	7800	2700	8000	8514	12300	8900
Specific heat	c [J(kgK)$^{-1}$]	860	740	960	440	431	213	411
Thermal conductivity	k [W(mK)$^{-1}$]	24.00	1	117.00	4.40	5.40	116.00	6.03
Thermal expansion	α [10^{-6}K^{-1}]	7.5	2.6	23.6	13.3	15	9.6	12.5

Material properties were taken from [19]

top surface of the planarized media is assumed to be flat as the continuous media as shown in Fig. 2(c).

Table I shows the material properties of the bulge and media used in this study [19]; those properties are assumed to be independent of temperature. A thermal-elastic-plastic material model described by Halquist [18] is adopted. Yielding occurs when the isotropic yield function is greater than zero

$$\phi = \frac{1}{2} S_{ij} S_{ij} - \frac{\sigma_Y^2}{3} \tag{2}$$

where S_{ij} is the deviatoric stress tensor and σ_Y is the yield strength in uniaxial tension. The stress is calculated based on the elastic and thermal strains.

III. NUMERICAL RESULTS AND DISCUSSIONS

A. Continuous Media

Fig. 3 shows the distribution of temperature rise of the continuous media at steady-state due to a 5-nm over-push of a bulge with $R = 2$ mm and $V = 10$ m/s. In this condition the friction is 0.7 mN, corresponding to a frictional heating of 7 mW, which is about 7% to 10% of the touchdown power of today's commercial heads. The maximum temperature rise is 17.2 K, which is substantial and may result in a sudden jump in temperature of a contact sensor, which may be used for contact detection [20], or a giant magnetoresistance (GMR) reader. Knigge *et al.* conducted touchdown experiments, and measured friction and GMR resistance. They observed that when the touchdown occurred, a rapid increase in GMR resistance by 0.20 to 0.25 Ohm, corresponding to a temperature rise of 6.7 °C to 8.4 °C, estimated from the known thermal coefficient of resistance [4]. It is noted that the measured GMR temperature rise was an average over the entire reader and may not be the maximum when contact occurred, and the tunnel magnetoresistance (TMR) reader used today is much less temperature-sensitive and, therefore, may not be a good means of detecting touchdown.

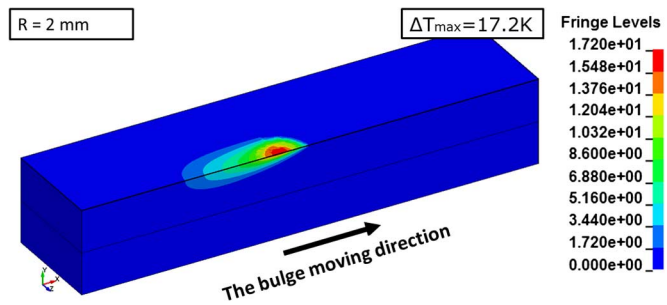

Fig. 3. Distribution of temperature rise at steady-state due to an over-push of 5 nm on the continuous media with $R = 2$ mm.

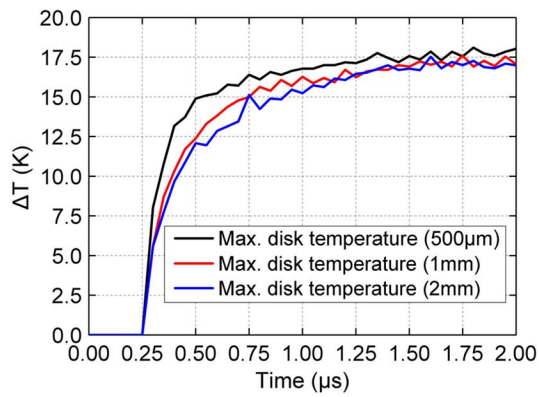

Fig. 4. Effect of bulge radius R on transient temperature rise for the continuous media. Indentation occurs from 0 to 0.25 μs with an over-push $\delta = 5$ nm followed by sliding at a constant velocity $V = 10$ m/s.

Fig. 4 shows the transient temperature rise at the contact interface during the touchdown process. The indentation occurs from 0 to 0.25 μs followed by the sliding from 0.25 μs. The temperature increases rapidly after the onset of the sliding, and it reaches a steady state without much oscillation. The peak temperature reaches 17 K and does not appear to depend on the bulge radius. Thermal time constant, defined as the time it takes to reach 63% of the steady-state temperature rise, is 120, 230, and 240 ns for a radius of 500 μm, 1 mm, and 2 mm, respectively.

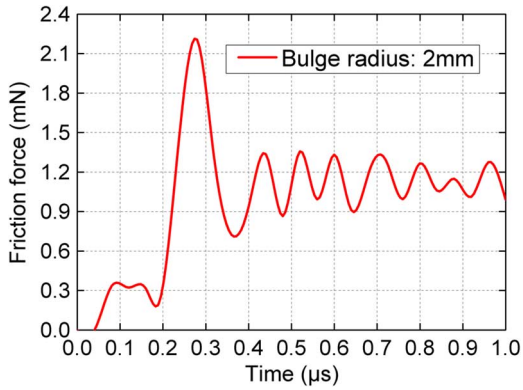

Fig. 5. Transient friction response of the touchdown process on the BPM ($\delta = 5$ nm and $V = 10$ m/s). Three stages are observed during the touchdown process: Stage 1 (indentation) from 0 to 0.05 μs, Stage 2 (initial sliding) from 0.05 μs to 0.4 μs, and Stage 3 (steady sliding) after 0.4 μs.

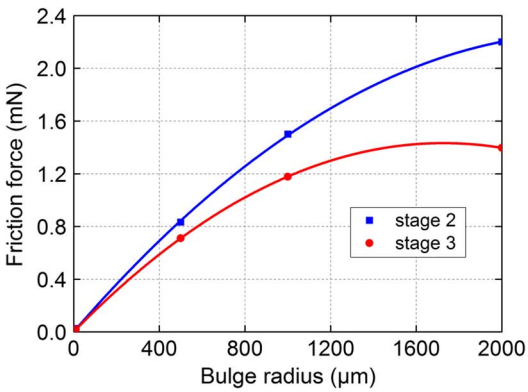

Fig. 6. Comparison of peak friction force between Stage 2 and Stage 3 as a function of bulge radius ($\delta = 5$ nm and $V = 10$ m/s).

We observe no plastic strain due to the touchdown process with a bulge radius from 500 μm to 2 mm. The simulation condition of 5 nm over-push and 10 m/s sliding velocity is considered severe. However, no plastic strain is observed for all bulge radii simulated, which means the continuous media exhibits less elastic and thermal stresses induced by the touchdown process, and hence is less likely to be damaged.

B. Bit-Patterned Media

The transient friction response of the touchdown process on the BPM is very different from the one on the continuous media as shown in Fig. 5. We observe three stages: Stage 1 (indentation) from 0 to 0.05 μs, Stage 2 (initial sliding) from 0.05 to 0.4 μs, and Stage 3 (steady sliding with oscillation) after 0.4 μs. The friction force is the maximum at the peak of Stage 2, and reaches a steady state with a constant mean and a considerable oscillation in Stage 3. Such distinctive phenomenon may be due to complex interaction between the bulge and the patterned surface. Fig. 6 shows a comparison of the peak friction force between Stage 2 and Stage 3 as a function of bulge radius. Both friction forces increase as the bulge radius increases when the over-push and sliding velocity are kept the same.

Fig. 7(a)–(d) shows detailed comparisons of temperature and plastic strain between Stage 2 and Stage 3 with a bulge radius of 2 mm, an over-push of 5 nm, and a sliding velocity of 10 m/s.

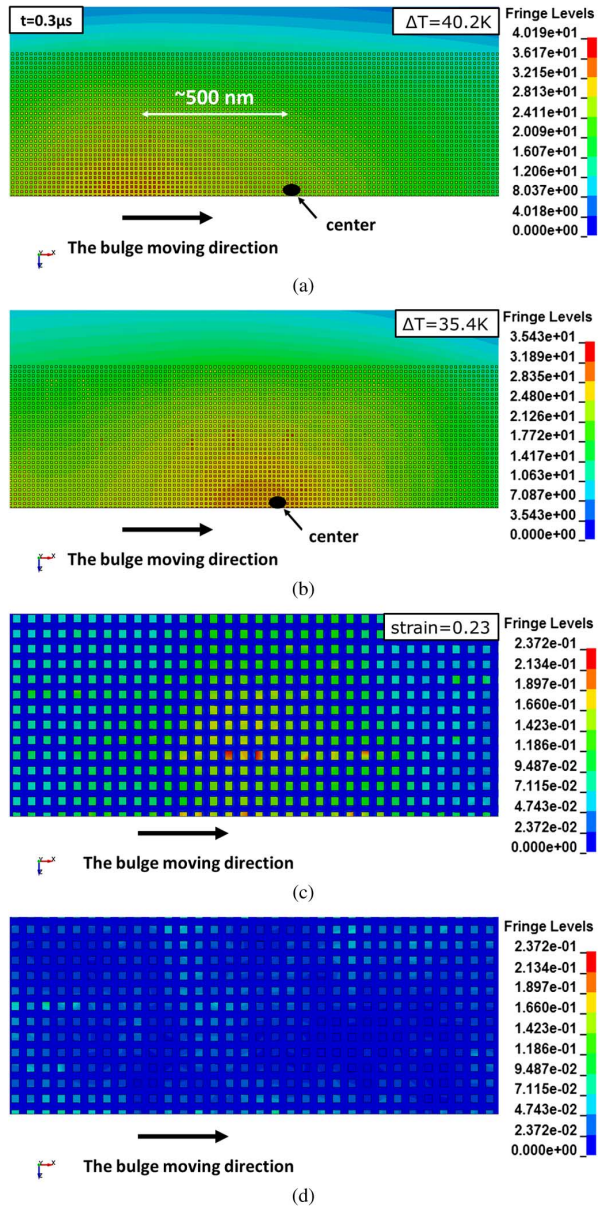

Fig. 7. Comparison of temperature and plastic strain between Stage 2 and Stage 3. (a) Temperature distribution at Stage 2. (b) Temperature distribution at Stage 3. (c) Plastic strain at Stage 2. (d) plastic strain at Stage 3 ($R = 2$ mm, $\delta = 5$ nm and $V = 10$ m/s).

The maximum temperature rises are 40.2 K and 35.4 K at Stage 2 and Stage 3, respectively, which are significantly higher than that on the continuous media. The temperature distributions appear circular with the maximum located along the plane of symmetry. At Stage 2 the center of the bulge is ahead of the location of maximum temperature by ~500 nm, whereas the distance is much smaller at Stage 3. Contrary to the continuous media, the touchdown process creates large plastic strains of 0.24 and 0.12 at Stage 2 and Stage 3, respectively. The plastic strain is irreversible, and can be catastrophic since the media may experience multiple touchdown calibrations in their lifetime. Besides, the distribution of plastic strain shows an irregular pattern distinct from the temperature. The maximum strain is not located on the plane of symmetry, and occurs at multiple locations as shown in Fig. 7(c) and (d).

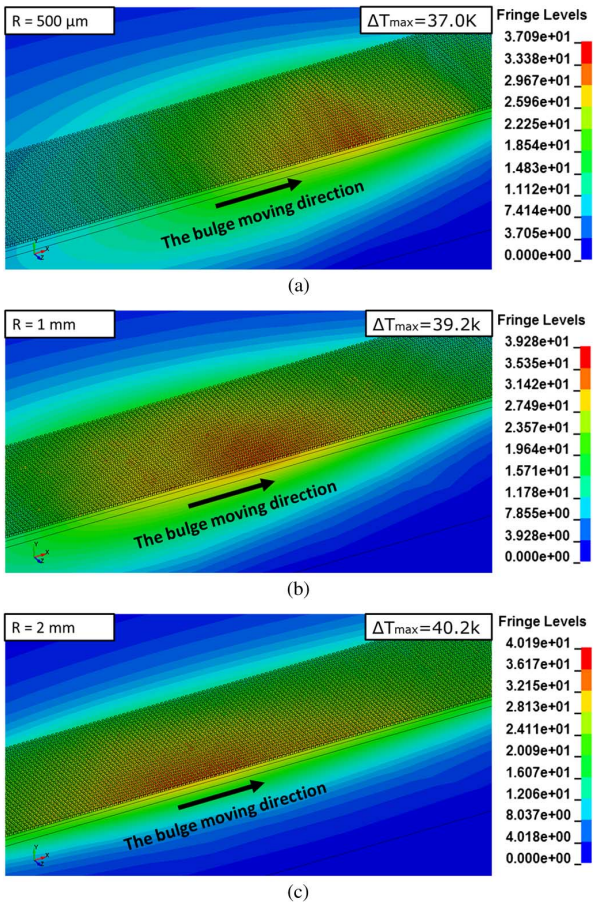

Fig. 8. Effect of bulge radius on temperature distribution for the BPM ($\delta = 5$ nm and $V = 10$ m/s). The center of the bulge is indicated in (c).

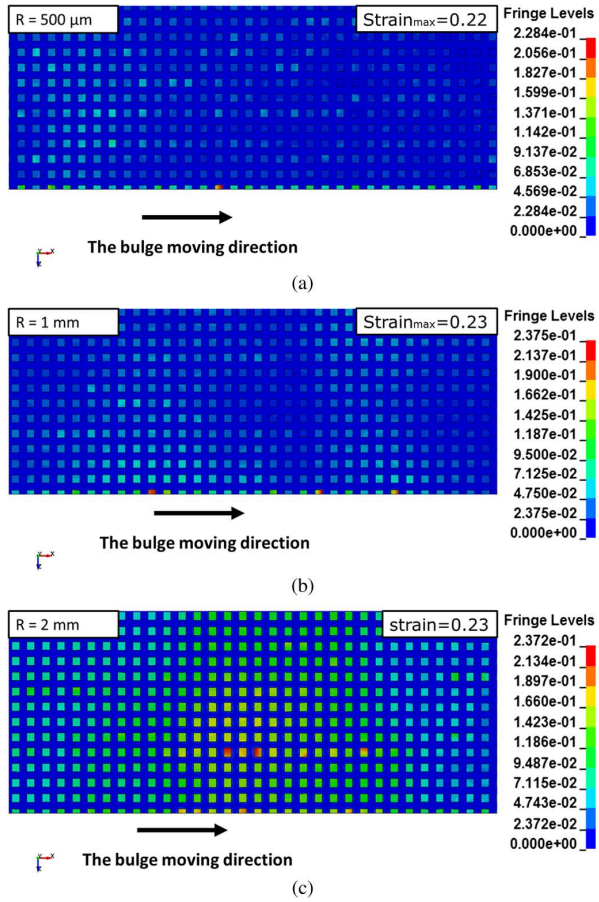

Fig. 9. Effect of bulge radius on plastic strain for the BPM ($\delta = 5$ nm and $V = 10$ m/s). The length in the x direction is approximately 650 nm.

Fig. 8(a)–(c) shows the effect of bulge radius on temperature rise. The maximum temperature increases by 8% as the bulge radius increases from 500 μm to 2 mm. Fig. 9 shows the effect of bulge radius on plastic strain. The maximum strain, generated at Stage 2, is 0.22 and is not dependent on the bulge radius. The area with plastic deformation increases with the bulge radius. It is intriguing that the plastic strain appears to exhibit some particular pattern unlike the expected spherical distribution of the temperature rise. We believe this is due to complicated interaction between the load, thermal stress, and isolated nanometer islands. Further study is required to understand the exact cause of the phenomenon.

C. *Effect of Planarization*

Since the patterned surface of BPM may cause instability of the air-bearing slider, planarization of BPM to produce a flat surface might be required. However, it is unclear what materials are preferable as the filling material, and how the planarization affects the media robustness to the touchdown process. In this session we carried out simulations to study the BPM planarized with SiO_2.

Fig. 10 shows the temperature distribution of planarized BPM with SiO_2. The simulation conditions are the same as those used for the unplanarized media shown in Fig. 8(c). The distribution exhibits an intriguing pattern distinct from those of the continuous media and unplanarized media, which suggests

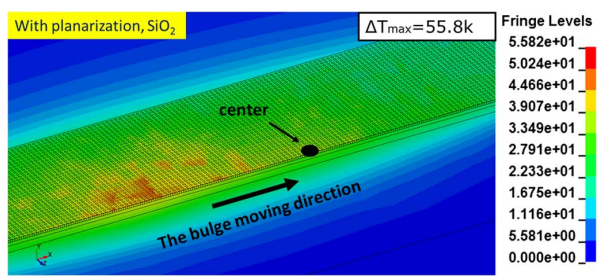

Fig. 10. Effect of planarization with SiO_2 on the temperature distribution of BPM ($t = 0.3$ μs, $\delta = 5$ nm, and $V = 10$ m/s). The center of bulge is indicated. The simulation conditions are the same as those used for the unplanarized media shown in Fig. 9(c).

that even though the planarized media has a flat surface, the inhomogeneous composition of materials significantly alters the heat conduction and, combined with the mismatch of coefficient of thermal expansion between SiO_2 and the recording material, produces an uneven media surface at the contact interface, which in turn makes the frictional heating more complicated.

Fig. 11 shows the effect of planarization on plastic strain. The maximum plastic strain is 0.37 compared to 0.23 in the unplanarized media shown in Fig. 9(c). The considerable increase in plastic strain indicates that planarization with SiO_2 degrades the media robustness to touchdown, and suggests that the selection of filling materials is crucial. The friction force response of the planarized BPM is similar to that of the unplanarized one as

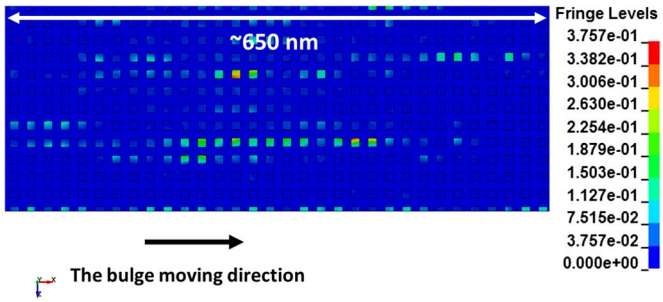

Fig. 11. Effect of planarization with SiO_2 on plastic strain of BPM ($\delta = 5$ nm and $V = 10$ m/s). The maximum plastic strain is 0.37 compared to 0.23 in the unplanarized media shown in Fig. 10(c). The simulation conditions are the same for both cases.

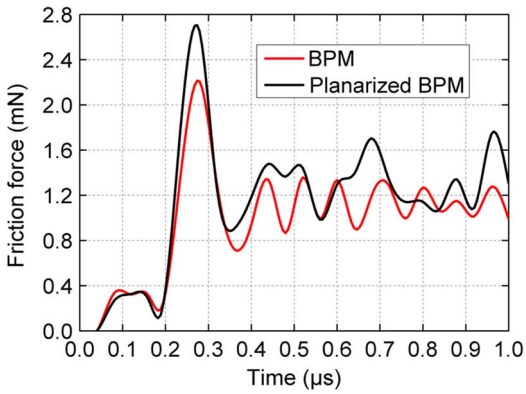

Fig. 12. Comparison of friction force response between BPM and planarized BPM ($\delta = 5$ nm and $V = 10$ m/s).

shown in Fig. 12, which implies that the media surface may be uneven at the contact interface due to the mismatch of thermal properties between SiO_2 and the recording material.

IV. Conclusion

We numerically study the impact of TFC touchdown on the continuous media, unplanarized BPM, and planarized BPM filling with SiO_2 by 3-D transient finite-element models with the frictional heating and thermal-elastic-plastic materials included. For continuous media, the touchdown condition with $R = 2$ mm, $\delta = 5$ nm, and $V = 10$ m/s does not create plastic strain, and the maximum temperature rise is approximately 17 K at a frictional heating of 7 mW. For unplanarized BPM, the same condition creates considerable plastic strain, and the maximum temperature reaches 40 K. Planarizing the BPM with SiO_2 significantly increases the plastic strain and temperature rise probably due to the mismatch of thermal properties between SiO_2 and the recording material, which suggests the selection of the filling material is crucial to the robustness of the BPM subjected to touchdown detection. Our study may also provide insights into the design of novel touchdown detection methods for BPM.

Acknowledgment

This work was supported in part by the National Science Council of Taiwan under Contract NSC 101-2221-E-002-151. The authors would like to thank Dr. A. Ovcharenko for helpful discussions on the finite-element model.

References

[1] J.-Y. Juang, J. Forrest, and F.-Y. Huang, "Magnetic head protrusion profiles and wear pattern of thermal flying-height control sliders with different heater designs," *IEEE Trans. Magn.*, vol. 47, no. 10, pp. 3437–3440, Oct. 2011.

[2] Q. H. Zeng, C.-H. Yang, S. Ka, and E. Cha, "An experimental and simulation study of touchdown dynamics," *IEEE Trans. Magn.*, vol. 47, no. 10, pp. 3433–3436, Oct. 2011.

[3] L. Su, Y. Hu, E. L. Lam, P. Li, R. W. Ng, D. Liang, O. Zheng, H. Liu, Z. Deng, and J. Zhang, "Tribological and dynamic study of head disk interface at sub-1-nm clearance," *IEEE Trans. Magn.*, vol. 47, no. 1, pp. 111–116, Jan. 2011.

[4] B. Knigge, T. Suthar, and P. Baumgart, "Friction, heat, slider dynamics during thermal protrusion touchdown," *IEEE Trans. Magn.*, vol. 42, no. 10, pp. 2510–2512, Oct. 2006.

[5] Y. Shimizu, J. Xu, H. Kohira, K. Kuroki, and K. Ono, "Experimental study on slider dynamics during touchdown by using thermal flying-height control," *Microsyst. Technol.*, vol. 17, pp. 897–902, Jun. 2011.

[6] N. Li, Y. Meng, and D. B. Bogy, "Experimental study of the slider-lube/disk contact state and its effect on head-disk interface stability," *IEEE Trans. Magn.*, vol. 48, no. 8, pp. 2385–2391, Aug. 2012.

[7] B. Liu, M. S. Zhang, S. K. Yu, W. Hua, Y. S. Ma, W. D. Zhou, L. Gonzaga, and Y. J. Man, "Lube-surfing recording and its feasibility exploration," *IEEE Trans. Magn.*, vol. 45, no. 2, pp. 899–904, Feb. 2009.

[8] B. D. Terris and T. Thomson, "Nanofabricated and self-assembled magnetic structures as data storage media," *J. Phys. D: Appl. Phys.*, vol. 38, pp. R199–R222, 2005.

[9] D. Weller and A. Moser, "Thermal effect limits in ultrahigh-density magnetic recording," *IEEE Trans. Magn.*, vol. 35, no. 6, pp. 4423–4439, Nov. 1999.

[10] E. E. Nunez, C.-D. Yeo, R. R. Katta, and A. A. Polycarpou, "Effect of planarization on the contact behavior of patterned media," *IEEE Trans. Magn.*, vol. 44, no. 11, pp. 3667–3670, Nov. 2008.

[11] J.-Y. Juang, D. Chen, and D. B. Bogy, "Alternate air bearing slider designs for areal density of 1 $\mathrm{Tb/in^2}$," *IEEE Trans. Magn.*, vol. 42, no. 2, pp. 241–246, Feb. 2006.

[12] J.-Y. Juang and D. B. Bogy, "Air-bearing effects on actuated thermal pole-tip protrusion for hard disk drives," *ASME J. Tribol.*, vol. 129, no. 3, pp. 570–578, Jul. 2007.

[13] T. Shiramatsu, M. Kurita, K. Miyake, M. Suk, S. O. H. Tanaka, and S. Saegusa, "Drive integration of active flying-height control slider with micro thermal actuator," *IEEE Trans. Magn.*, vol. 42, no. 10, pp. 2513–2515, Oct. 2006.

[14] J. Zheng, D. B. Bogy, S. Zhang, and W. Yan, "Effects of altitude on thermal flying-height control actuation," *Tribol. Lett.*, vol. 40, no. 3, pp. 295–299, Feb. 2010.

[15] N. Liu, J. Zheng, and D. B. Bogy, "Thermal flying-height control sliders in hard disk drives filled with air-helium gas mixtures," *Appl. Phys. Lett.*, vol. 95, p. 213505, 2009.

[16] J.-Y. Juang, T. Nakamura, B. Knigge, Y. Luo, W.-C. Hsiao, K. Kuroki, F.-Y. Huang, and P. Baumgart, "Numerical and experimental analyses of nanometer-scale flying height control of magnetic head with heating element," *IEEE Trans. Magn.*, vol. 44, no. 11, pp. 3679–3682, Nov. 2008.

[17] [Online]. Available: http://www.lstc.com/lsdyna.htm

[18] J. O. Hallquist, LS-DYNA Theoretical Manual. Livermore, CA, USA, Livermore Software Technol. Corp., 2006.

[19] A. Ovcharenko, M. Yang, K. Chun, and F. E. Talke, "Simulation of magnetic erasure due to transient slider-disk contacts," *IEEE Trans. Magn.*, vol. 46, no. 3, pp. 770–777, Mar. 2010.

[20] Y. Shimizu, J. Xu, H. Kohira, M. Kurita, T. Shiramatsu, and M. Furukawa, "Nano-scale defect mapping on a magnetic disk surface using a contact sensor," *IEEE Trans. Magn.*, vol. 47, no. 10, pp. 3426–3432, Oct. 2011.